Conformational Plasticity in Broadly Neutralizing HIV-1 Antibodies Triggers Polyreactivity

Julie Prigent, Annaëlle Jarossay, Cyril Planchais, Caroline Eden, Jérémy Dufloo, Ayrin Kök, Valérie Lorin, Oxana Vratskikh, Thérèse Couderc, Timothée Bruel, et al.

Article

Cell Reports

Conformational Plasticity in Broadly Neutralizing HIV-1 Antibodies Triggers Polyreactivity

Graphical Abstract

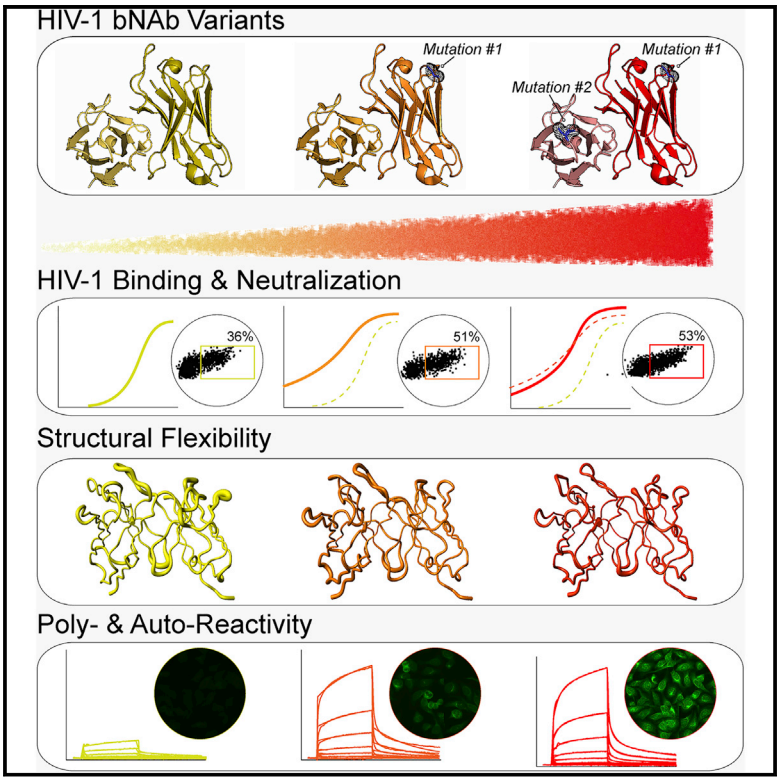

Highlights

- Most HIV-1 bNAbs are polyreactive and often cross-react with self-antigens
- Polyreactivity of bNAbs involves hydrophobic interactions
- Mutations enhancing HIV-1 bNAbs' capacities also induce *de novo* polyreactivity
- Enhanced neutralization and polyreactivity co-emerge by antibody conformational flexibility

Authors

Julie Prigent, Annaëlle Jarossay, Cyril Planchais, ..., Oliver Ohlenschläger, Jordan D. Dimitrov, Hugo Mouquet

Correspondence

oliver.ohlenschlaeger@leibniz-fli.de (O.O.), jordan.dimitrov@crc.jussieu.fr (J.D.D.), hugo.mouquet@pasteur.fr (H.M.)

In Brief

HIV-1 bNAbs are frequently polyreactive and bind to self-antigens. Prigent et al. show that specific mutations in bNAbs that enhance their neutralizing capacity create an intrinsic structural flexibility of the antibody paratope. This promotes the conformational adaptation that facilitates binding to HIV-1 variants and polyreactivity to topologically distinct non-HIV-1 molecules.

Prigent et al., 2018, Cell Reports *23*, 2568–2581
May 29, 2018
https://doi.org/10.1016/j.celrep.2018.04.101

CellPress

OPEN ACCESS
CellPress

Cell Reports
Article

Conformational Plasticity in Broadly Neutralizing HIV-1 Antibodies Triggers Polyreactivity

Julie Prigent,[1,2,13] Annaëlle Jarossay,[3,4,5,13] Cyril Planchais,[1,2,13] Caroline Eden,[6,7] Jérémy Dufloo,[8,9] Ayrin Kök,[1,2] Valérie Lorin,[1,2] Oxana Vratskikh,[1,2] Thérèse Couderc,[10] Timothée Bruel,[8,9] Olivier Schwartz,[8,9] Michael S. Seaman,[11] Oliver Ohlenschläger,[12,*] Jordan D. Dimitrov,[3,4,5,*] and Hugo Mouquet[1,2,14,*]

[1]Laboratory of Humoral Response to Pathogens, Department of Immunology, Institut Pasteur, Paris 75015, France
[2]INSERM U1222, Paris 75015, France
[3]Sorbonne Universités, UPMC Univ Paris 06, UMR_S 1138, Centre de Recherche des Cordeliers, Paris 75006, France
[4]INSERM, UMR_S 1138, Centre de Recherche des Cordeliers, Paris 75006, France
[5]Université Paris Descartes, Sorbonne Paris Cité, UMR_S 1138, Centre de Recherche des Cordeliers, Paris 75006, France
[6]Laboratory of Molecular Immunology, The Rockefeller University, New York, NY 10065, USA
[7]Icahn School of Medicine at Mount Sinai, New York, NY 10029, USA
[8]Virus & Immunity Unit, Department of Virology, Institut Pasteur, Paris 75015, France
[9]CNRS URA3015, Paris 75015, France
[10]Biology of Infection Unit, INSERM U1117, Department of Cell Biology and Infection, Institut Pasteur, Paris 75015, France
[11]Beth Israel Deaconess Medical Center, Boston, MA 02215, USA
[12]Leibniz Institute on Aging - Fritz Lipmann Institute, Jena 07745, Germany
[13]These authors contributed equally
[14]Lead Contact
*Correspondence: oliver.ohlenschlaeger@leibniz-fli.de (O.O.), jordan.dimitrov@crc.jussieu.fr (J.D.D.), hugo.mouquet@pasteur.fr (H.M.)
https://doi.org/10.1016/j.celrep.2018.04.101

SUMMARY

Human high-affinity antibodies to pathogens often recognize unrelated ligands. The molecular origin and the role of this polyreactivity are largely unknown. Here, we report that HIV-1 broadly neutralizing antibodies (bNAbs) are frequently polyreactive, cross-reacting with non-HIV-1 molecules, including self-antigens. Mutating bNAb genes to increase HIV-1 binding and neutralization also results in *de novo* polyreactivity. Unliganded paratopes of polyreactive bNAbs with improved HIV-1 neutralization exhibit a conformational flexibility, which contributes to enhanced affinity of bNAbs to various HIV-1 envelope glycoproteins and non-HIV antigens. Binding adaptation of polyreactive bNAbs to the divergent ligands mainly involves hydrophobic interactions. Plasticity of bNAbs' paratopes may, therefore, facilitate accommodating divergent viral variants, but it simultaneously triggers promiscuous binding to non-HIV-1 antigens. Thus, a certain level of polyreactivity can be a mark of adaptable antibodies displaying optimal pathogens' recognition.

INTRODUCTION

The humoral arm of the immune system relies on the remarkable variety of immunoglobulin molecules (or antibodies) expressed as receptors on B cells or secreted in body fluids, which ensure the recognition of a theoretically infinite number of foreign antigens. This diversity results mainly from the random rearrangement of germline V(D)J genes coding for the immunoglobulin heavy- and light-chain variable domains (Tonegawa, 1983), which associate to form the antigen-binding site or paratope. The primary antibody repertoire is further broadened by the conformational malleability of germline-encoded paratopes that permits low-affinity-binding adaptation to structurally distinct molecules (Kaur and Salunke, 2015). Adaptive immune responses naturally occurring upon infection or induced by vaccination generate high-affinity antibodies to culprit antigens and memory B cell subsets to respond to further antigenic challenges. Upon antigen encounter in secondary lymphoid organs, special microenvironments called germinal centers (GCs) form and support the clonal expansion, maturation, and affinity-based selection of B cells (Victora and Nussenzweig, 2012). In GCs, B cells undergo somatic hypermutation (SHM) of immunoglobulin (Ig) genes that potentially increases antibody affinity to the target antigen (Victora and Nussenzweig, 2012). Concomitantly, antibody paratopes of matured B cells tend to lose the flexibility characterizing polyspecific unmutated B cell precursors and rigidify, allowing optimal contacts with cognate antigens (Jimenez et al., 2003; Kaur and Salunke, 2015; Wedemayer et al., 1997; Yin et al., 2003; Zimmermann et al., 2006). Class-switched memory B cells shaped during GC reactions to express high-affinity Ig can acquire poly- and self-reactivity, which are normally counterselected by tolerance mechanisms during B cell ontogeny (Goodnow et al., 2005; Koelsch et al., 2007; Prigent et al., 2016; Tiller et al., 2007; Wardemann and Nussenzweig, 2007). *De facto*, serological antibody polyreactivity is commonly associated with several human infections (Mouquet and Nussenzweig, 2012), and high-affinity human antibodies to diverse pathogens, including *Plasmodium falciparum* (Muellenbeck et al., 2013), influenza virus (Andrews et al., 2015), and HIV-1 (Liu et al., 2015; Mouquet and Nussenzweig, 2012; Mouquet et al., 2010), are also frequently polyreactive.

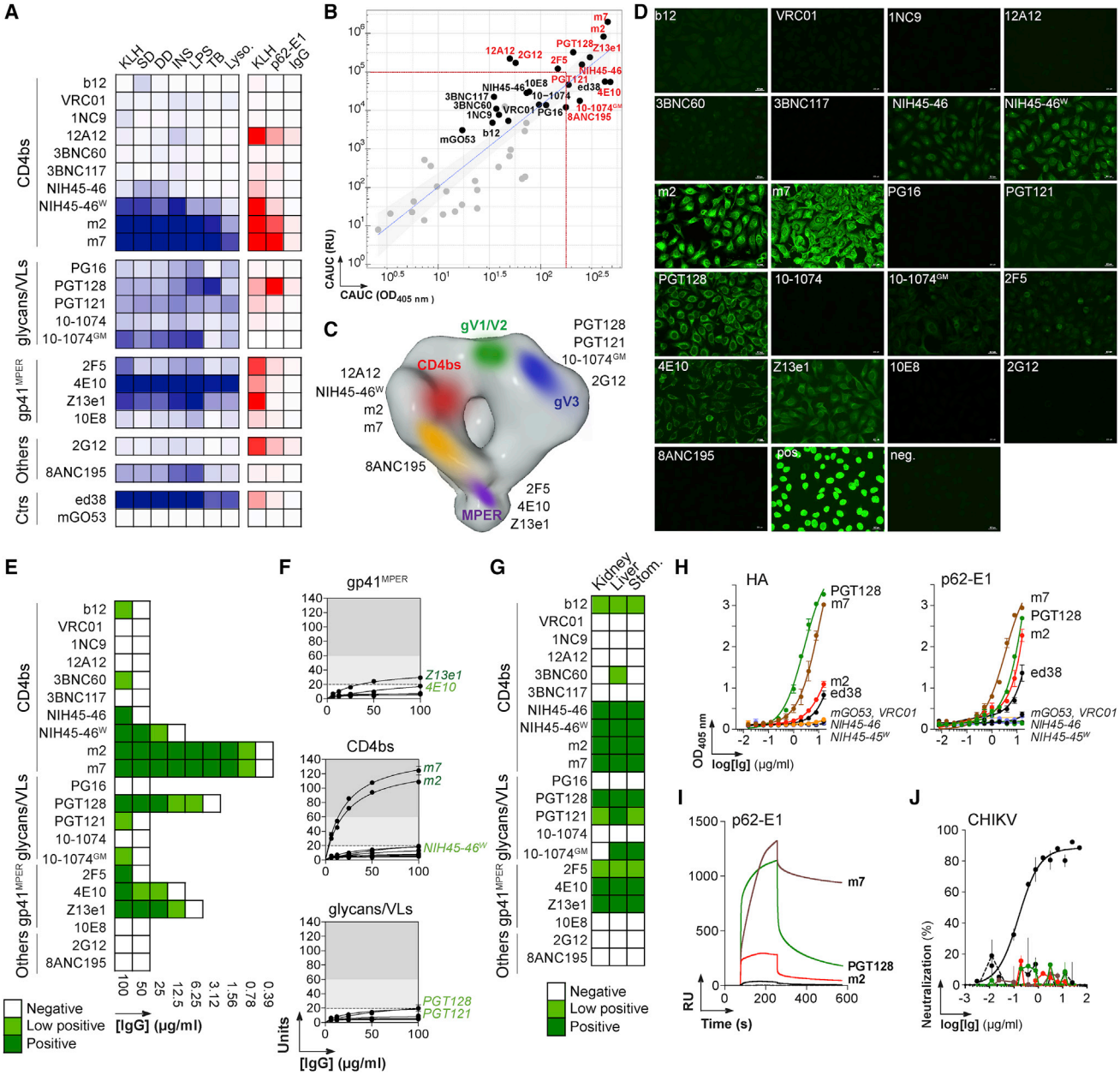

Figure 1. Poly- and Self-Reactivity of HIV-1 bNAbs

(A) Heatmap showing the antibody binding to the selected antigens as measured by ELISA (blue) and surface plasmon resonance (SPR) (red) in Figure S1. Color intensity is proportional to the reactivity level with darker colors indicating high binding while light colors show moderate binding (white, no binding). KLH, keyhole limpet hemocyanin; SS and DS, single- and double-stranded DNA; INS, insulin; LPS, lipopolysaccharide; TB, thyroglobulin; Lyso., lysozyme; p62-E1, Chikungunya virus (CHIKV) Env protein; IgG, human immunoglobulin G.

(B) Linear regression plot comparing the binding values obtained by ELISA and SPR for KLH alone (gray dots) and for all tested antigens (black dots). Polyreactive bNAbs are depicted in red.

(C) Schematic diagram of HIV-1 envelope glycoprotein showing the epitopes of polyreactive bNAbs.

(D) Antibody binding to HEp-2 cells assayed by immunofluorescence assay (IFA) with all bNAbs at 100 μg/mL.

(E) Titration of HEp-2 IFA reactivity as shown in (D).

(F) Graphs show ELISA binding curves of HIV-1 bNAbs against HEp-2 lysate antigens.

(G) Heatmap showing the IFA reactivity of HIV-1 bNAbs to antigens expressed by mouse kidney, liver, and stomach (Stom.).

(H) ELISA graphs show the binding of PGT128, m2, and m7 to purified Influenza hemagglutinin (HA, left) and Chikungunya virus (CHIKV) p62-E1 (right) glycoproteins.

(legend continued on next page)

Neutralizing antibodies to HIV-1 target the surface envelope glycoprotein (gp160) (Levy, 1998), and, among them, particular antibodies are able to neutralize most HIV-1 strains (Mouquet, 2014). Several unusual but essential Ig features characterize these HIV-1 broadly neutralizing antibodies (bNAbs), e.g., high load of SHM, nucleotide insertions or deletions (indels), long and tyrosine-rich CDR_H3, some of which are associated with antibody polyreactivity (Haynes et al., 2005; Liao et al., 2011, 2013). Polyreactivity may confer them with a selective advantage for viral binding (Mouquet et al., 2010) and neutralization (Alam et al., 2009; Mouquet et al., 2012b; Scherer et al., 2010). Immune tolerance control may, however, limit or block the development of bNAbs with exacerbated cross-reactivity to self-antigens (Chen et al., 2013; Kelsoe and Haynes, 2017; Schroeder et al., 2017; Verkoczy et al., 2010, 2011; Zhang et al., 2016). Importantly, bNAbs possess prophylactic and therapeutic capacities for preventing and treating HIV-1 infection (Mouquet, 2014), and they are thought to be mandatory mediators of potentially successful HIV-1 vaccines (Mouquet, 2015). Therefore, elucidating the molecular mechanisms linking the acquisition of bNAb activity with poly-/auto-reactivity is essential to better appreciate whether polyreactivity contributes to HIV-1 neutralization or is simply a bystander effect of affinity maturation. Notably, knowing whether the conformational flexibility typical of germline B cell precursors is also responsible for the dual recognition of HIV-1 Env and non-HIV-1 antigens by highly matured bNAbs is key in the comprehension of this phenomenon.

Here we show that most HIV-1 bNAbs are polyreactive. Certain bNAbs have Ig gene mutations enhancing HIV-1 cross-binding and -neutralization capacities but concomitantly creating *de novo* polyreactivity. Using binding affinity, thermodynamic, and molecular dynamics analyses, we report that the co-emergence of enhanced neutralizing capacities and polyreactivity is due to an intrinsic conformational flexibility of the antigen-binding sites of bNAbs, which allows a better accommodation of divergent HIV-1 Env variants.

RESULTS

High Prevalence of Polyreactive HIV-1 bNAbs Reacting with Self-Antigens

Polyreactivity is a common feature of HIV-1 antibodies (Mouquet et al., 2010), and it was also reported for some HIV-1 bNAbs (Haynes et al., 2005; Liu et al., 2015). To evaluate the poly- and auto-reactivity of HIV-1 bNAbs, 21 IgG antibodies from 14 independent B cell clonal lineages, targeting all pan-neutralizing gp160 epitopes and including naturally occurring as well as artificially improved IgG molecules (Supplemental Experimental Procedures), were assayed in multiple antigen-binding assays. Half of the antibodies exhibited medium-to-high polyreactivity against various non-HIV antigens by ELISA (Figures 1A, S1A, and S1B). Polyreactivity of HIV-1 bNAbs was verified by surface plasmon resonance (SPR)-binding analyses (Figures 1A, S1C, and S1D), which strongly correlated with ELISA reactivity profiles (Figure 1B). Combining both assays, 57% of HIV-1 bNAbs were polyreactive, including prototypic polyspecific anti-MPER 2F5 and 4E10 (Haynes et al., 2005) but also antibodies targeting all sites of vulnerability of the HIV-1 envelope spike (Figure 1C). Interestingly, all rationally designed bNAbs, but only one-third of naturally occurring potent HIV-1 neutralizers, showed polyreactivity.

To determine whether HIV-1 bNAbs could cross-react against self-antigens, we performed indirect immunofluorescence assay (IFA) and ELISA analyses on HEp-2 cells, which are routinely used in clinical autoantibody assays. Almost all polyreactive bNAbs showed low to high binding of HEp-2 antigens (Figure 1D), with 4E10, Z13e1, NIH45-46^W, PGT128, m2, and m7 being the most reactive (Figures 1E and 1F). The self-reactivity of IgG bNAbs was also evidenced by positive IFA staining on kidney, liver, and/or stomach tissues (Figure 1G). SPR experiments showed that some polyreactive bNAbs also recognized viruses other than HIV-1 (Figure S1C). Indeed, PGT128, m2, and m7 strongly reacted against the envelope proteins of Influenza and Chikungunya (CHIK) viruses (Figure 1H). Although HIV-1 bNAbs displayed non-negligible apparent affinity to CHIK viral glycoproteins (Figure 1I), they were unable to neutralize CHIK virus (CHIKV) *in vitro* using luciferase-expressing virus and classical plaque neutralization assays (Figures 1J and S1E).

We conclude that a majority of HIV-1 bNAbs harbors polyreactive behavior. The most reactive are rationally designed molecules and naturally occurring antibodies interacting with epitopes combining protein moieties and membrane lipids (e.g., 4E10 and 2F5) or envelope carbohydrates (e.g., PGT128 and PGT121). High polyreactivity of bNAbs generally translates into cross-reactivity to self- and non-HIV viral antigens, which may imply the recognition of ubiquitous host components (carbohydrates and lipids).

bNAb Variants Harbor Heterogeneous Polyreactivity Profiles

NIH45-46^W, m2, and m7 were engineered from the VRC01 class CD4bs bNAb NIH45-46 (Scheid et al., 2011) to improve their *in vitro* neutralization activity and *in vivo* protective efficacy (Diskin et al., 2011, 2013). NIH45-46^W has a single substitution in its CDR_H2 loop (IgH^{G54W}) filling up the gp120 Phe^{43} cavity, which normally engages the Phe^{43} of CD4 molecules, thereby enhancing both affinity and neutralization potency (Diskin et al., 2011) (Figure 2A). Neutralization breadth of NIH45-46^W was further extended by adding in the antibody's CDR_L1 loop the IgL^{S28Y} mutation, which enables the NIH45-46m2 variant (m2) to interact with the $gp120^{N276}$-attached glycan (Diskin et al., 2013) (Figure 2A). A third variant, NIH45-46m7 (m7), was engineered by introducing a second IgH substitution (W47V) to confer neutralization against NIH45-46^W-resistant and/or

(I) SPR sensorgram shows the binding of PGT128, m2, and m7 to purified p62-E1. Green (dotted) and black lines show binding of non-polyreactive mGO53 and polyreactive ED38 control antibodies, respectively.

(J) Graphs comparing the *in vitro* neutralization activities of PGT128, m2, and m7 against CHIKV (La Réunion strain). Green and black dotted lines show the negative (mGO53) and positive anti-CHIKV control antibodies, respectively. Errors bars in (F), (H), and (J) indicate the SEM of duplicate values.

See also Figure S1.

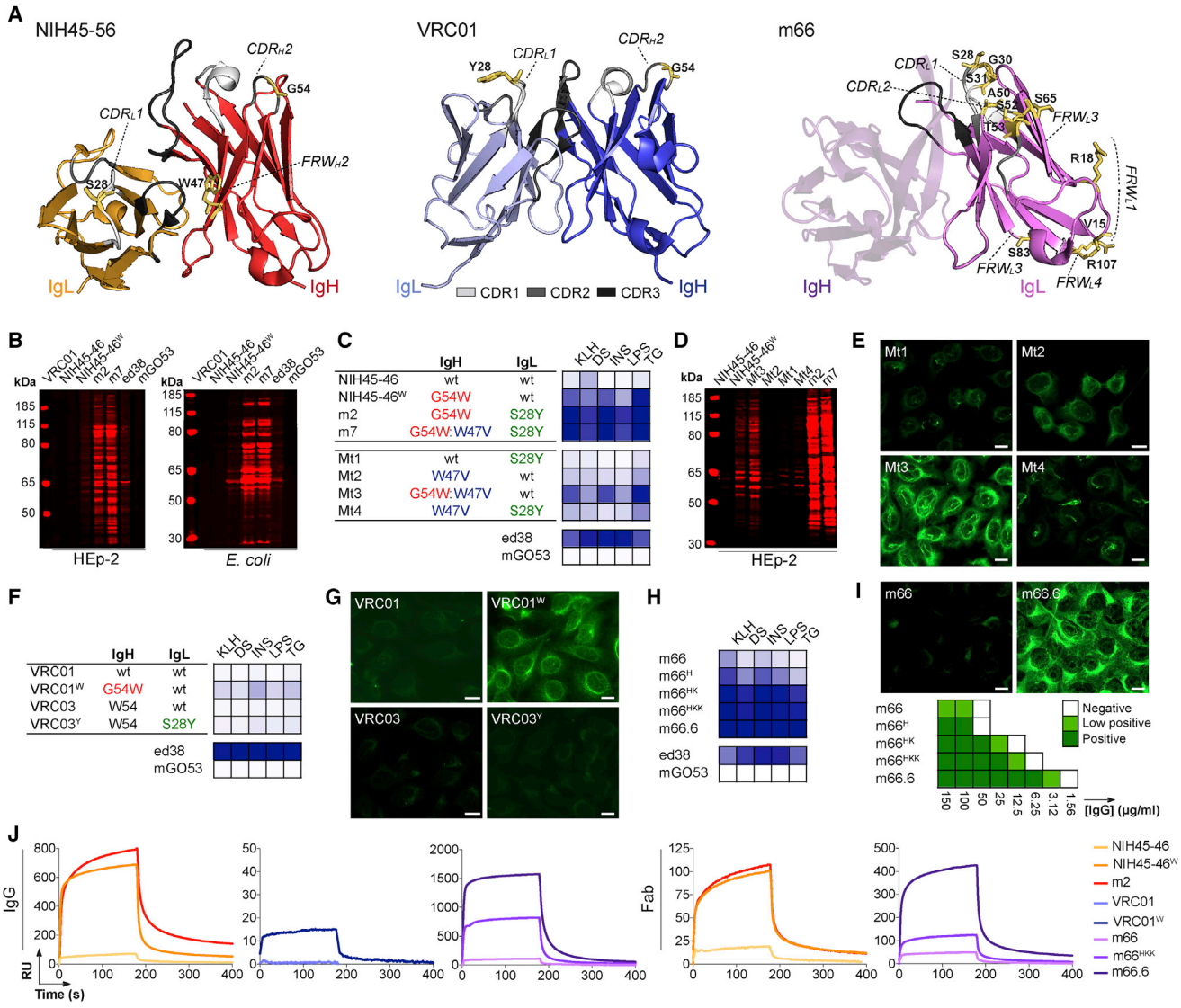

Figure 2. Poly- and Self-Reactivity of bNAb Variants

(A) Ribbon diagrams showing the crystal structures of NIH45-46 (PDB: 3U7W), VRC01 (PDB: 3NGB), and m66 variable domain (PDB: 4NRY). Amino acid residues distinguishing bNAb variants are depicted as yellow sticks. The complementary determining regions (CDRs) and framework regions (FRWs) in which these mutations are located are indicated on each structure.

(B) Polyreactive binding of rationally designed NIH45-46 antibody variants and controls (20 μg/mL) was assayed by immunoblot analyses on HEp-2 and *E. coli* protein extracts. Representative infrared scans from two independent experiments are shown.

(C) Table shows all combinations of three amino acid substitutions (IgH^{W47V}, IgH^{G54W}, and IgL^{S28Y}) in NIH45-46 mutant antibodies (left). Heatmap compares the ELISA binding of the selected antibodies to various antigens as measured in Figure S2 (right). KLH, keyhole limpet hemocyanin; DS, double-stranded DNA; INS, insulin; LPS, lipopolysaccharide; TG, thyroglobulin.

(D) Immunoblotting on HEp-2 protein extract comparing the polyreactive binding of novel NIH45-46 mutant (mt1 to mt4) and control antibodies. Representative infrared scans from two independent experiments are shown.

(E) HEp-2 reactivity of NIH45-46 mt1-mt4 antibodies was evaluated by IFA. Representative IFA images from two independent experiments are shown.

(F) Same as for (B) but for VRC01/3 and mutant antibodies.

(G) Same as for (D) but for VRC01/3 and mutant antibodies.

(H) Heatmap comparing the ELISA binding of the selected antibodies to various antigens as measured in Figure S2.

(I) HEp-2 reactivity of m66 and m66.6 (100 μg/mL) was evaluated by IFA (top). Heatmap shows titration of HEp-2 IFA reactivity for m66 antibody variants (bottom).

(J) Binding of selected IgG bNAbs and corresponding Fabs to KLH was evaluated by SPR analysis as shown in Figure S2I. The y axis shows the response units (RUs) obtained at a given time (s, seconds) indicated on the x axis.

See also Figure S2.

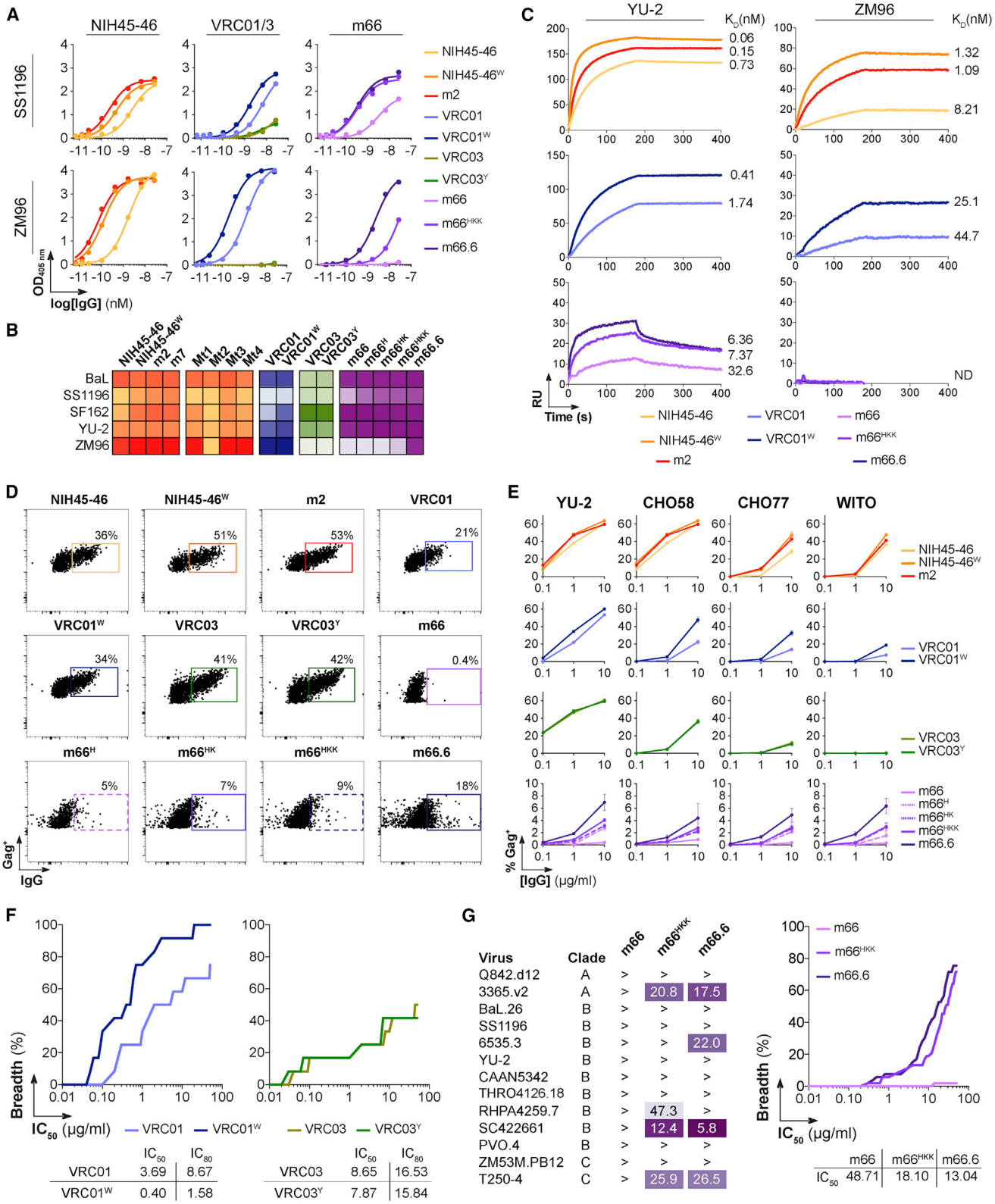

Figure 3. HIV-1 Binding and Neutralization by bNAb Variants

(A) ELISA graphs comparing the binding of selected bNAbs to trimeric SS1196 and ZM96 gp140 glycoproteins. Error bars indicate the SEM of duplicate or triplicate $OD_{405\ nm}$ values from 1 to 2 experiments.

(legend continued on next page)

escape mutant strains (Diskin et al., 2013) (Figure 2A). Strikingly, we observed a gradual increase of poly- and self-reactivity levels following the accumulation of substitutions in NIH45-46 (m7 > m2 > NIH45-46^{W} > NIH45-46) (Figures 1 and S1). Immunoblot analyses on total HEp-2 and *E. coli* proteins also revealed increasing numbers of immunoreactive antigens (m7/m2 > NIH45-46^{W} > NIH45-46) (Figures 2B and S2A), suggesting a simultaneous augmentation of polyreactivity strength and spectrum.

To identify the contribution of single versus combined substitutions (IgH^{W47V}, IgH^{G54W}, and IgL^{S28Y}) in enhanced polyreactivity, we generated a series of NIH45-46 variants (Mt1 to Mt4) comprising all combinations of unique and double mutations (Figure 2C). Neither IgL^{S28Y} and IgH^{W47V} alone nor combined promoted high polyreactive binding (Figures 2C–2E and S2D). Although 45-46 Mt3, which has both IgH mutations (W47V and G54W), had a slight increase of poly- and self-reactivity compared to NIH45-46^{W}, the magnitude of binding was much lower than for m2 (IgH^{G54W} and IgL^{S28Y}) (Figures 2C–2E). Thus, the IgH^{G54W} mutation promoted the appearance of polyreactivity, but its association with IgL^{S28Y} in m2 amplified the binding to non-HIV-1 ligands, suggesting a synergetic effect of these two mutations for the induction of polyspecificity. NIH45-46 shares 85% and 52% IgH sequence identity (96% and 61% for IgL) with its clonal variants VRC01 and VRC03, respectively. Interestingly, compared to NIH45-46, VRC01 and VRC03 naturally possess IgL^{S28} and IgH^{W54} residues, respectively (Figure 2A). To test whether the IgH^{W54}/IgL^{S28} combination could confer polyreactivity to VRC01 and VRC03, we generated two new mutants, VRC01^{G54W} (VRC01^{W}) and VRC03^{S28Y} (VRC03^{Y}). Interestingly, VRC01^{W}, but not VRC03^{Y}, exhibited *de novo* poly- and auto-reactive binding compared to its wild-type counterpart (Figures 2F, 2G, S2E, and S2F). Thus, as previously shown for VRC07 (Rudicell et al., 2014), the IgH^{W54} mutation can potentiate for polyreactivity in NIH45-46 clonal variants, but only when IgH and IgL genes are not too divergent.

Anti-MPER m66 and m66.6 are clonally related antibody variants. Both antibodies differ in terms of neutralization potency and breadth but also poly- and self-reactivity; m66.6, but not m66, is a broad neutralizer and highly polyspecific (Zhu et al., 2011). We thus evaluated the polyreactive pattern of m66, m66.6, and three mutant antibodies with amino acid substitutions in the m66 CDR$_L$1 loop; m66^{H} (m66 IgL^{S28H}), m66^{HK} (m66 IgL$^{S28H-G30K}$), and m66^{HKK} (m66 IgL$^{S28H-G30K-S31K}$) (Figure 2A), which displayed intermediate neutralization activity (Ofek et al., 2014). We observed a gradual increase of poly-/self-reactivity according to the number of amino acid substitutions (m66.6 > m66^{HKK} > m66^{HK} > m66^{H} > m66) (Figures 2H, 2I, S2G, and S2H). SPR-binding experiments confirmed that both IgG and Fabs of polyreactive antibody variants have an increased apparent affinity to exogenous non-HIV ligands when compared to non-polyreactive bNAbs (Figures 2J and S2I).

In sum, polyreactivity qualitatively and quantitatively varies among members of bNAbs' B cell lineages. This variation is due to a handful of IgH and IgL residues located outside the antigen-binding loops, which trigger polyreactivity when engrafted into non-polyreactive clonal variants.

Polyreactivity Co-emerges with Enhanced Antibody Cross-Reactivity and -Neutralization of HIV-1

Rationally designed NIH45-46 antibodies and m66 variants are known to possess superior Env-binding affinity and neutralization potency and breadth compared to their parental bNAbs (Diskin et al., 2011, 2013). To further evaluate the extent of enhanced HIV-1 Env cross-reactivity, we measured the binding of NIH45-46, VRC01/3, and m66 IgG variants to five different trimeric gp140 glycoproteins by ELISA. We observed a gradual increase of the apparent affinity to HIV-1 Env across antibody variants (Figures 3A, 3B, and S3A), which followed the magnitude of polyreactivity (Figure 2). For instance, augmented binding for NIH45-46 engineered variants (m7/m2 > NIH45-46^{W} > NIH45-46) and VRC01^{W}, but not VRC03^{Y}, was evidenced for 4 of 5 gp140 strains. Comparably, polyreactive m66 antibody variants (m66.6 > m66^{HKK} > m66^{HK} and m66^{H} > m66) showed increased reactivity against 3 of the 5 Env proteins (Figures 3A, 3B, S3A, and S3B). SPR analyses performed on YU-2 and ZM96 trimer-immobilized chips confirmed the higher affinity to HIV-1 Env of most polyreactive IgG antibodies (Figures 3C and S3C). Accordingly, mutated variants of NIH45-46, VRC01, and m66, but not VRC03, also displayed enhanced binding to HIV-1 Env exposed at the surface of infected cells (Figures 3D, 3E, and S3D).

Augmented neutralization potency and breadth of NIH45-46^{W} and m2 and m7 were linked to an increased affinity and slower off-rates (Diskin et al., 2011, 2013). We asked whether VRC01^{W} exhibits enhanced neutralization properties against a cross-clade panel of 12 HIV-1 isolates, when compared to VRC01. VRC01^{W} was more potent (geometric mean IC$_{50}$ =

(B) Heatmap shows the antibody binding to various trimeric HIV-1 gp140 proteins as measured by ELISA in Figure S3. Color intensity is proportional to the reactivity level with darker colors indicating high binding while light colors show moderate binding.
(C) SPR sensorgrams comparing the binding of selected IgG bNAbs to trimeric YU-2 and ZM96 gp140 glycoproteins (as shown in Figure S3C).
(D) Cytograms show a representative binding of bNAb IgGs to Gag^{+} YU-2-infected cells.
(E) Graph comparing percentage of binding of bNAb variants to selected viral strains exposed at the surface of infected target cells, as measured by flow cytometry (as shown in D). Error bars indicate the SEM of triplicate percent values from 2 independent experiments.
(F) Coverage graph comparing the neutralization breadth and potencies of VRC01, VRC03, and mutant antibodies evaluated in triplicate by TZM-bl assay against a panel of 12 viruses, as shown in Figure S3E. IC$_{50}$ and IC$_{80}$ geometric means are indicated in the table below.
(G) Neutralization activity of m66 variants. Table shows the neutralization activity of the selected IgG against a panel of selected pseudoviruses used in the TZM-bl assay. Values correspond to IC$_{50}$s measured in duplicate. Greater than symbol (>) indicates that the IC$_{50}$ for a given virus was not reached at the maximum concentration tested (50 μg/mL). Coverage graph (right) compares the neutralization breadth and potency of m66 and antibody variants, combining previously published data on 40 viral strains (Ofek et al., 2014) and those obtained using the TZM-bl assay against a novel panel of 13 viruses (left). IC$_{50}$ and IC$_{80}$ geometric means are indicated in the table below.
See also Figure S3.

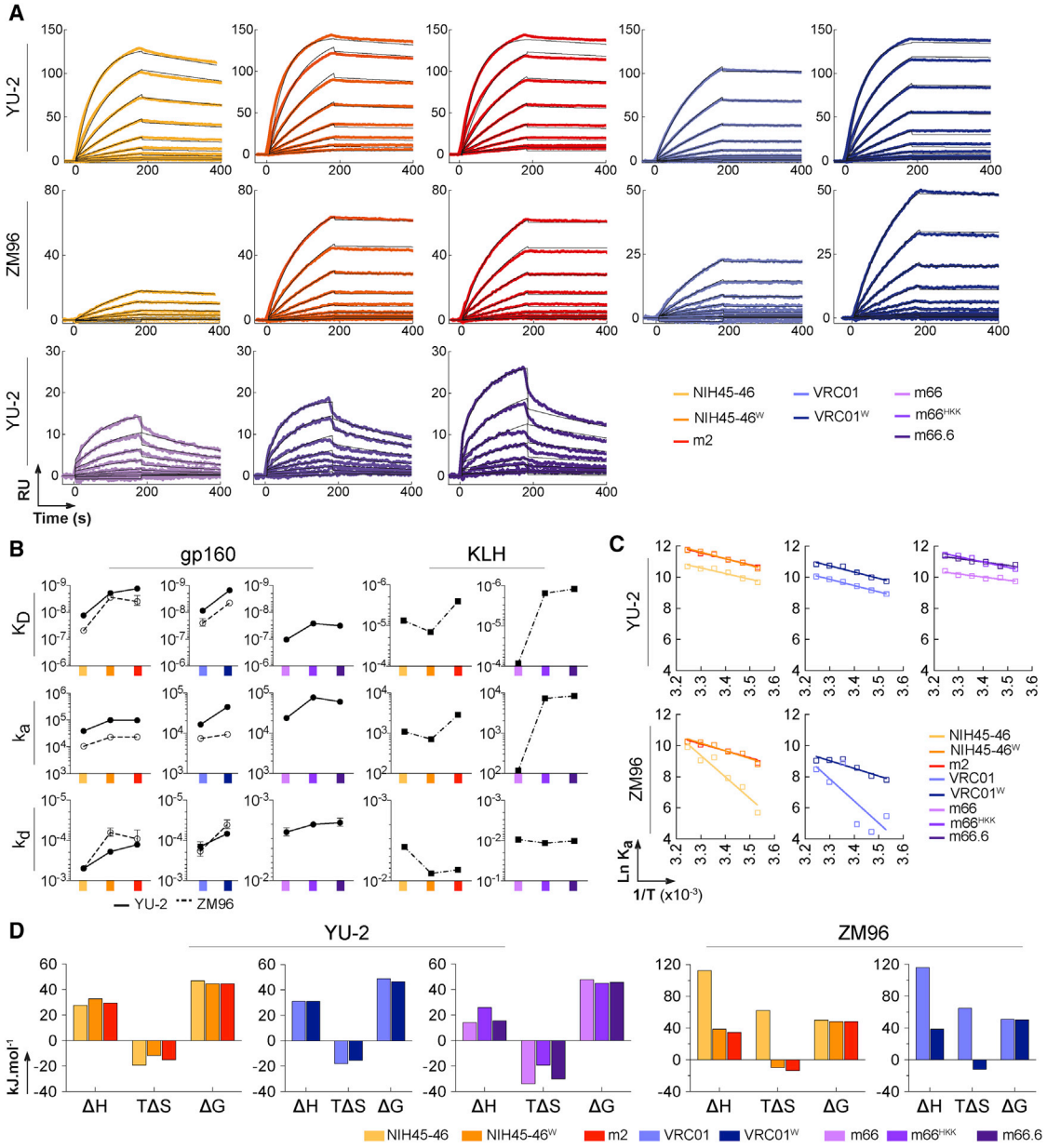

Figure 4. Binding Affinity and Thermodynamics of bNAbs' Fabs

(A) SPR sensorgrams comparing the binding of the Fabs of selected bNAbs to immobilized trimeric YU-2 and ZM96 gp140 glycoproteins.

(B) Graphs comparing the relative affinity (K_D) and kinetics constants (k_a and k_d) of bNAbs' Fabs to trimeric gp140 glycoproteins (YU-2 and ZM96) and KLH, as measured from (A).

(C) Arrhenius plots show the temperature dependence of the association binding constant of Fabs to trimeric YU-2 and ZM96 gp140 glycoproteins.

(D) Bar graph comparing the changes in thermodynamic parameters calculated by Eyring's analyses using slopes of Arrhenius plots depicted in (C).

See also Figure S4.

0.40 versus 3.69 μg/mL for VRC01) and broader, with 100% of the panel's viruses neutralized, while only 75% were sensitive to VRC01 (Figures 3F and S3E). On the other hand, the presence of the IgL^{S28Y} mutation in VRC03 did not improve neutralization (geometric mean IC_{50} = 7.87.40 versus 8.65 μg/mL for VRC03 and $VRC03^{Y}$, respectively) (Figures 3F and S3E). Finally, combining already published and new *in vitro* neutralization data, we confirmed that m66.6 and $m66^{HKK}$ have comparable neutralization activities, which largely surpassed the one of the m66 antibody (Figure 3G) (Ofek et al., 2014; Zhu et al., 2011).

Overall, our data show that the most polyreactive variants of various bNAbs also display broad Env cross-reactivity and enhanced neutralization breadth and potency.

Polyreactive bNAb Variants Display Conformational Adaptation upon HIV-1 Env Binding

To gain insights into the mechanisms of polyreactivity-associated HIV-1 Env cross-reactivity, we performed kinetic and thermodynamic analyses of monovalent interactions by SPR using bNAbs' Fabs. Real-time binding data revealed that NIH45-46, VRC01, and respective mutants interact with high affinity with both YU-2 and ZM96 HIV-1 gp140 trimers. In contrast, Fabs of m66 and its variants bound only to YU-2 gp140 (Figure 4A). Evaluation of the kinetic rate constants (k_a and k_d) and the equilibrium dissociation constant (K_D) confirmed that mutations that augmented polyreactivity also increased the affinity of bNAbs for YU-2 and ZM96 gp140 proteins (Figure 4B). For all bNAb variants, higher binding affinities were due to synergistic changes in the kinetic rate constants. Thus, compared to their wild-type counterparts, NIH45-46, VRC01, and m66 variants displayed both increased association to gp140 ligands and decreased dissociation (Figures 4A and 4B). We then performed kinetic analyses on the binding of bNAbs' Fabs to the non-cognate antigen KLH. Improved affinity of polyreactive variants against KLH was mostly due to a faster association for m2, $m66^{HKK}$, and m66.6 and to a slower dissociation for $NIH45\text{-}46^{W}$ (Figures 4B and S2I).

To examine more precisely the molecular mechanisms responsible for the dual recognition of HIV-1 and non-HIV antigens by prototypic bNAbs and their polyreactive variants, we next performed thermodynamic analyses by measuring binding kinetics as a function of the temperature. We focused our analyses on the association phase, as it strongly depends on conformational changes in the interacting partners. For all bNAb Fabs binding to YU-2 trimers, an increase in temperature correlated with a concomitant rise in the association rates (Figures 4C and S4). Mutations amplifying bNAbs' polyreactivity had no influence on the temperature sensitivity of the association rate constant, as deduced by almost identical slopes of the Arrhenius plots (Figure 4C). However, antibodies exhibited a distinct behavior when binding to ZM96 gp140. The association rates of NIH45-46 and VRC01 Fabs to ZM96 had a pronounced sensitivity to temperature, which is typical of interactions made by pre-formed binding sites (lock-and-key binding model; Manivel et al., 2000). Interestingly, polyreactive mutants of NIH45-46 and VRC01 lost sensitivity to elevated temperatures (Figure 4C).

We next derived activation energies and thermodynamic parameters that characterized the protein-protein interactions from Arrhenius plots. We observed identical qualitative changes of the activation enthalpy ($\Delta H^{\ddagger}$) and the activation entropy ($T\Delta S^{\ddagger}$) during the association of wild-type and mutant Fabs to YU-2 gp140 (Figure 4D). $\Delta H^{\ddagger}$ and $T\Delta S^{\ddagger}$ were respectively positive and negative, indicating that those changes had unfavorable contributions to the overall binding energy of all bNAbs. Activation thermodynamic changes showed distinct trends when considering the antibody association to ZM96 trimers; NIH45-46 and VRC01 presented contrasting qualitative changes of $T\Delta S^{\ddagger}$ as compared to their mutant counterparts. The interactions of parental antibodies with ZM96 were characterized by positive $T\Delta S^{\ddagger}$, but polyreactive mutant bNAbs displayed negative $T\Delta S^{\ddagger}$ values (Figure 4D). Also, although changes in $\Delta H^{\ddagger}$ remained positive, absolute values for polyreactive mutants decreased about 3-fold compared to parental bNAbs (Figure 4D). The detected high favorable values of $T\Delta S^{\ddagger}$ (>40 kJ/mol) indicated that binding of NIH45-46 and VRC01 to ZM-96 Env protein was accompanied by an increase in the disorder of the system, most probably mediated by a disruption of ordered solvent shells surrounding interacting proteins. These changes in the association energetics are consistent with the interactions of rigid antibody-binding sites. In contrast, negative $T\Delta S^{\ddagger}$ values observed for polyreactive bNAbs suggest that, upon complex formation, the net disorder in the system decreases. This may be explained by a reduction in the intrinsic conformational freedom in the proteins, and it suggests the presence of conformational adaptations upon formation of the intermolecular complexes.

Hydrophobic Interactions Enhance Affinity of Polyreactive bNAbs to HIV-1 Env

Changes in $\Delta H^{\ddagger}$ (the heat absorbed or released by the system) depend on the nature and the quantity of non-covalent contacts between interacting molecular surfaces. To provide a better explanation for the marked decrease of $\Delta H^{\ddagger}$ characterizing the binding of polyreactive bNAbs to ZM96 HIV-1 trimers, we analyzed the non-covalent forces involved in the formation of the complexes. First, we compared the hydrophobicity of Fab fragments of bNAbs and their variants by using a fluorescent probe. Mutations in bNAbs, associated with both an increase in HIV-1 Env cross-reactivity and polyreactivity toward various non-HIV-1 antigens, did not change the overall hydrophobicity of the Fabs (Figure 5A). We then analyzed the antibody binding to various HIV-1 Env and non-HIV polyreactive antigens as a function of the ionic strength. The interactions of IgG bNAbs with gp120/gp140 glycoproteins and polyreactive ligands were sensitive to changes in the ionic environment, as evidenced by the decreased ELISA reactivity with increased salt concentrations (Figure 5B). This is consistent with the implication of polar bonds in the complexes' formation. Of note, polyreactive variants were not sensitive to ionic strength or much less than their parental counterparts (Figure 5B). This suggests that hydrophobic interactions were the main driving force involved in the complexes' formation. Thus, introducing mutations that allow for enhanced HIV-1 cross-binding and -neutralization as well as *de novo* polyreactivity qualitatively changed the type of non-covalent forces from polar to non-polar. This may provide an explanation for the significant drop in $\Delta H^{\ddagger}$ values.

Collectively, these results suggest that mutations in bNAbs augmenting cross-Env-binding affinity and neutralizing activity and polyreactivity are associated with enhanced structural dynamics of the antibody paratope. These mutations also change the type of non-covalent forces driving the formation of antigen-bNAb complexes.

Polyreactive HIV-1 bNAbs with Enhanced Neutralization Display Paratope Conformational Flexibility

To better understand the conformational adaptation of certain bNAbs upon binding to HIV-1 Env and non-HIV antigens, we explored changes in structural dynamics of parental and mutated antibody paratopes using molecular dynamic (MD) simulations. MD analyses performed in parallel for NIH45-46, $NIH45\text{-}46^{W}$, and m2 showed that introduction of the single

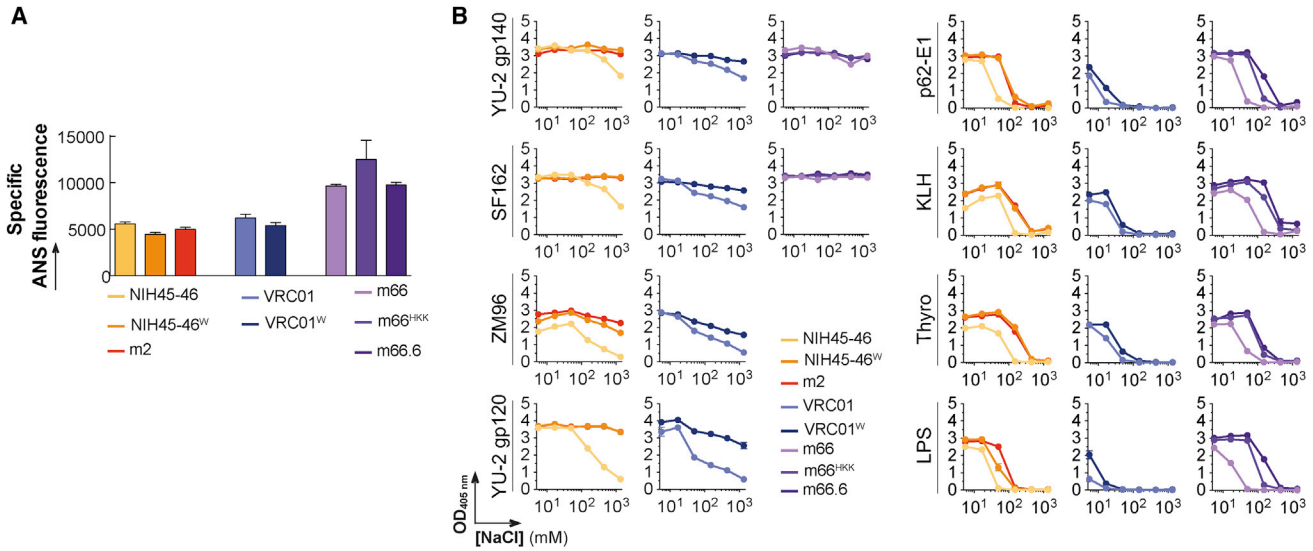

Figure 5. Hydrophobic Interactions in bNAbs' Binding to HIV-1 Env and Non-HIV-1 Antigens

(A) Bar graphs comparing the overall hydrophobicity of Fabs of selected bNAbs, as measured by fluorescence spectroscopy using anilinonaphthalene-8-sulfonic acid (8-ANS) dye. Error bars indicate the SD of replicate values (n = 5).

(B) The ionic strength dependence of the binding of IgG antibodies to HIV-1 Env glycoproteins and non-HIV antigens was evaluated by ELISA. Error bars indicate the SEM of duplicate $OD_{405\ nm}$ values. Thyro, thyroglobulin.

IgH^{G54W} mutation decreased the total energy of the antibody structure (Figures 6A and S5A). Adding the second mutation in the light chain, IgL^{S28Y}, led to a drastic drop in the total energy of the molecular system (Figures 6A and S5A). Both mutations affected the molecular flexibility of the respective chains. An increase in the root-mean-square (RMS) values reflecting the dynamics of the IgH was noticed for NIH45-46^{W} compared to the parental bNAb (2.40 versus 1.90 Å in NIH45-46), while the additional mutation in m2 increased the IgL RMS values from 1.44 to 1.66 Å (Figures 6B, 6C, and S5B). The overall RMS values considering IgH and IgL chains of NIH45-46 antibody variants were stable in the range of 2.2 Å (Figure 6B). The trajectory of the $VRC01^{W}$, which has the IgH^{G54W} mutation in association with a naturally present Tyrosine residue in position 28 of the IgL, closely resembled that observed for the analogous m2 antibody, with low total energies (Etot $\sim -9.5 \times 10^4$ kcal/mol) and RMS values around 1.49 Å (Figures 6A–6C and S5). Here the IgH^{G54W} exchange resulted in an energetic drop (Figures 6A and S5A). This indicates that the major changes in the molecular dynamics were mainly due to the interplay between antibody variable domains, each with the mutated site. A similar tendency, albeit not as pronounced as for NIH45-46/VRC01, was observed for m66-derived antibodies. Both m66.6 and $m66^{HKK}$ mutant exhibited higher total energies compared to m66 ($\sim -9 \times 10^4$ versus -10.5×10^4 kcal/mol) (Figures 6A and S5A). Moreover, the flexibility of the whole antibody reflected in the total RMS showed higher and similar values, respectively, for $m66^{HKK}$ and m66.6 as compared to m66 (1.85 and 1.80 Å versus 1.64 Å, respectively) (Figures 6B, 6C, and S5). However, the m66.6 IgL exhibited a considerably lower flexibility (Figure S5; Table S1) than m66 and $m66^{HKK}$, suggesting that the additional mutations in m66.6 could counterbalance the flexibility effect induced by $H^{28}K^{30}K^{31}$ mutations. Structural features further support this as the $H^{28}K^{30}K^{31}$ mutations in the CDR_H1 loop were located close to the CDR_H2 loop harboring $G^{50}L^{52}N^{53}$ residues, which also distinguished both antibody variants (Figure S6). In addition, the higher flexibility of m66.6 within the m66 family can be attributed to motional contributions of the common IgH.

We conclude that specific mutations create an intrinsic structural flexibility of the antigen-binding site of certain bNAbs, which promotes the conformational adaptation facilitating binding to HIV-1 Env variants and polyreactivity.

DISCUSSION

HIV-1 bNAbs are likely key effectors of protective HIV-1 vaccines. However, their induction by immunization remains difficult as they are naturally elicited from complex co-evolution host-pathogen processes, which are not yet fully resolved (Victora and Mouquet, 2018). Immune tolerance control represents one of the putative roadblocks preventing the selection of bNAb-expressing B cell clones when they express highly poly-/auto-reactive B cell receptors (BCRs) (Kelsoe and Haynes, 2017; Verkoczy et al., 2017).

In this study, we investigated the polyreactive properties of natural and artificially engineered HIV-1 bNAbs. Combining various immunoassays, we show that almost 60% of the tested HIV-1 bNAbs exhibited low to high polyreactivity. This is in agreement with a former estimation of polyreactive HIV-1 bNAbs (Liu et al., 2015; Verkoczy and Diaz, 2014). We further revealed a previously unappreciated polyreactive binding for PGT121, PGT128, NIH45-46^{W}, m2, and m7. The magnitude of polyreactivity differed among antibodies from low to high binders, with only a few being highly cross-reacting with

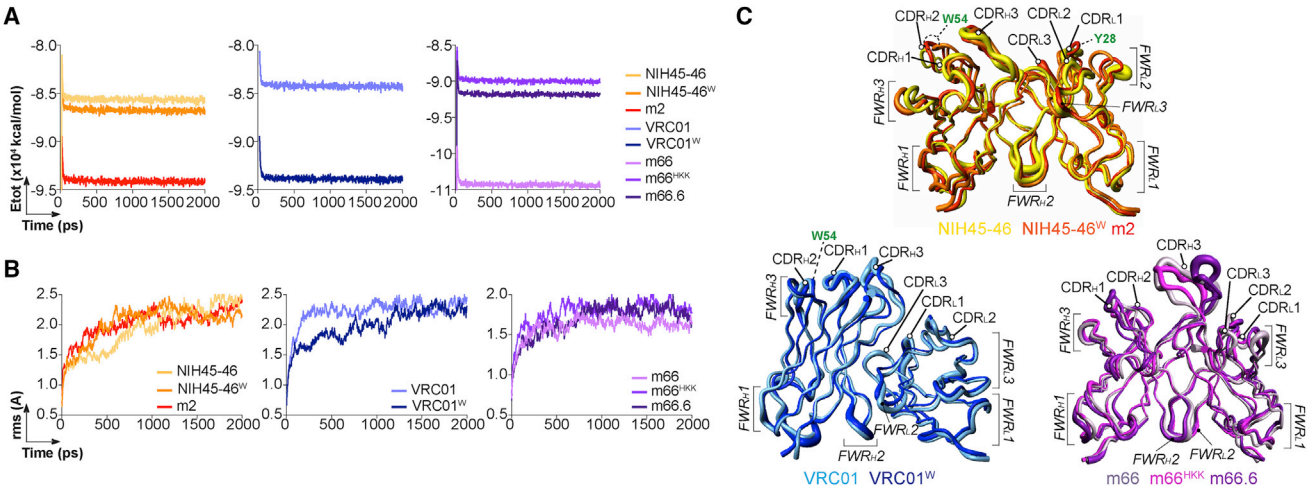

Figure 6. Conformational Flexibility of HIV-1 bNAbs' Antigen-Binding Sites

(A) Graph comparing the total energy profile of bNAbs' antigen-binding sites (ABSs) overtime during the MD simulations.

(B) Graph comparing the root-mean-square (RMS) deviation of all atoms in bNAbs' ABSs during the MD run.

(C) Putty ribbon diagrams comparing local RMS displacements during the MD run. Structures of bNAbs' variants are superimposed.

See also Figures S5 and S6 and Table S1.

autoantigens (e.g., 4E10, m2 and m7, and m66.6). Abnormally high polyreactivity was commonly found in rationally engineered and phage display-derived bNAbs, which could be explained by the absence of natural counterselection by *in vivo* tolerance mechanisms. Single mutations in more potent engineered variants of VRC07 and 10E8 have been previously shown to create *de novo* poly- and cross-reactivity (Kwon et al., 2018; Rudicell et al., 2014). This may limit the use of these types of antibodies as immunotherapeutics, due to their short half-life as evidenced *in vivo* (Rudicell et al., 2014; Shingai et al., 2013, 2014). However, strategies aiming at eliminating (e.g., by *N*-glycans engraftment) and selecting for a lack of binding promiscuity (by screening methods) gave rise to enhanced mutants with no or tolerable polyreactivity (Chuang et al., 2015; Jardine et al., 2016; Kwon et al., 2018), which could be more safely evaluated in clinical trials. In infected humans, B cells expressing poly- and self-reactive bNAbs could be proscribed by diverse tolerance mechanisms (Kelsoe and Haynes, 2017; Verkoczy et al., 2017). Thus, even if not pathogenic, self-reactivity of bNAbs could interfere with their development upon infection or vaccination (Kelsoe and Haynes, 2017; Verkoczy et al., 2017). Whether most HIV-1 bNAbs, which display no or only moderate promiscuous binding, are also subjected to immune tolerance control remains to be explored (Mouquet, 2014). Conversely, relaxed or defective tolerance may certainly facilitate bNAbs' induction (Bonsignori et al., 2016; Schroeder et al., 2017). This led to envisioning various strategies to overcome tolerance control over bNAbs' induction upon vaccination (Kelsoe and Haynes, 2017; Verkoczy et al., 2017). Strikingly, polyreactivity can naturally arise in parallel with enhanced HIV-1 binding and neutralization during affinity maturation, but the most potent antibody variants are not always polyspecific (Bonsignori et al., 2016; Liao et al., 2011, 2013). Hence, affinity-enhancing mutations do not always lead to polyreactivity, and, even so, compensatory mutations could possibly suppress polyreactivity and/or stabilize antibody structure (in case of a deleterious mutation), allowing affinity and breadth gain without counterselection. We showed nonetheless here that specific Ig mutations confer simultaneously enhanced HIV-1 binding affinity and neutralization and polyreactivity for bNAb variants to the CD4bs and MPER epitopes. Similarly, hydrophobic residues of 2F5 and 4E10 CDR_H3 loops interacting with membrane lipids, and likely involved in their polyspecificity, are required for neutralization (Alam et al., 2007, 2009; Scherer et al., 2010). Our data also show that particular mutations can supply bNAb variants with a coincident gain of HIV-1 binding affinity, neutralization capacities, and promiscuous reactivity to numerous non HIV-1 antigens. Thus, polyreactivity seems to be intimately linked to the functional properties of some HIV-1 bNAbs, as previously demonstrated with HIV-1 antibodies capable of heteroligation (Mouquet et al., 2010). It will be of interest to determine whether the links between polyreactivity and neutralization that we describe here also occur with bNAbs targeting epitopes other than the CD4bs and MPER.

The capacity of germline-encoded B cell precursors to accommodate topologically dissimilar antigens with low affinity has been linked to the conformational flexibility of their antibody paratope (Adhikary et al., 2012; Khan and Salunke, 2014; Manivel et al., 2000, 2002; Thielges et al., 2008; Wedemayer et al., 1997). Conformational plasticity can also be found in affinity-matured antibodies, including antiviral bNAbs. One such antibody, H5.3, a potent H5N1 influenza neutralizer, undergoes conformational change upon binding to the H5 subunit, which also implies peripheral interactions to polymorphic residues (Winarski et al., 2015). Our thermodynamics and MD analyses suggest that intrinsic conformational flexibility enabled higher affinity variants of HIV-1 bNAbs to bind divergent HIV-1 Env and non-HIV antigens. Promiscuous binding to disparate

antigens involves the flexibility of the antibody paratope and binding plasticity through a modulation of hydrophobic interactions (Krishnan et al., 2007, 2008; Tapryal et al., 2013). Indeed, hydrophobic interactions greatly contribute to the enhanced binding of bNAbs' variants to divergent HIV-1 Env and polyreactive ligands, most likely by stabilizing antibody-antigen complexes (Li et al., 2003; Mohan et al., 2003, 2009; Rajpal et al., 1998; Sundberg et al., 2000).

Our observations are reminiscent of those described for murine monoclonal antibodies to hen white-egg lysozyme (HEL). In these studies, the SHM-derived increased affinity of anti-HEL antibodies was associated with decreased thermostability and increased conformational flexibility of the binding sites, which formed plastic hydrophobic bonds with mimetic antigens (Acchione et al., 2009; Mohan et al., 2003, 2009; Sinha et al., 2002). Thus, we hypothesize that the paratope plasticity of HIV-1 bNAbs provides sufficient flexibility to accommodate subtle epitopic variations in divergent HIV-1 Env, as previously suggested for anti-HIV-1 gp41 peptide antibodies (Bhowmick and Salunke, 2013). For instance, conformational flexibility may help m66.6 accommodating different MPER conformers. During B cell ontogeny, increased affinity and flexibility of the antigen-binding site can be accompanied by a gain of auto-reactivity, as shown for HIV-1 bNAb 4E10 (Finton et al., 2014). Acquisition of poly- and auto-reactivity occurs during the affinity maturation toward neutralization breadth of both gp41- and gp120-specific B cells (Liao et al., 2011, 2013). This phenomenon could originate from the selection of clones with more plastic antigen-binding sites. On the other hand, in agreement with the paradigm of paratope rigidification upon affinity maturation (Jimenez et al., 2003; Manivel et al., 2000; Schmidt et al., 2013; Wedemayer et al., 1997; Zimmermann et al., 2006), the accumulation of SHM in HIV-1 bNAbs can optimize paratope complementarity with Env and restrict structural motility (Davenport et al., 2016). Therefore, affinity maturation of B cells likely selects for high affinity antibodies with either lock-and-key preconfigured binding sites or intrinsic flexibility by modeling paratope, as proposed earlier (Mohan et al., 2003).

In summary, enhanced binding and neutralization abilities of HIV-1 bNAbs are often linked to the recognition of non-HIV-1 antigens. This promiscuous reactivity can be input into the binding sites' flexibility, triggered by SHMs, which aid in accommodating not only divergent HIV-1 Env glycoproteins but also topologically distinct non-HIV-1 molecules via plastic hydrophobic structural interfaces. Thus, affinity maturation of HIV-1-reactive B cells toward neutralizing breadth may be tightly regulated between the selection of clones with adaptable antibody-binding sites for an expanded HIV-1 recognition and the counterselection by immune tolerance of highly polyreactive clones reacting with self-antigens. It is tempting to speculate that this phenomenon may occur with other pathogens with diversifying antigens, making antibodies' natural development or elicitation by vaccines particularly difficult.

EXPERIMENTAL PROCEDURES

Recombinant HIV-1 Proteins and Antibodies

Recombinant human IgG1 antibodies, Fab molecules, and gp140 proteins were produced by co-transfection of FreeStyle 293-F cells (Fisher Scientific) using the polyethylenimine (PEI)-precipitation method and purified as previously described (Lorin and Mouquet, 2015; Mouquet et al., 2012a). See the Supplemental Experimental Procedures for further details.

Poly- and Auto-reactivity Assays

Polyreactivity, HEp-2 and viral envelope-specific ELISAs, and HEp-2 IFAs were performed as previously described (Prigent et al., 2016). SPR-binding experiments were performed as previously described (Mouquet et al., 2010). Polyreactivity was also evaluated by infrared immunoblotting on HEp-2 cell and *E. coli* protein extracts. See the Supplemental Experimental Procedures for further details.

Viral Binding and Neutralization Assays

Antibody binding to viruses on infected cells was assayed by flow cytometry as recently described (Bruel et al., 2016). Neutralization of cell-free HIV-1 was measured using TZM-bl cells as previously described (Li et al., 2005; Lorin et al., 2017). To assay for CHIKV neutralization, luciferase-based and plaque neutralization assays were used, as described in the Supplemental Experimental Procedures.

SPR Affinity and Thermodynamic Analyses

The apparent affinity of HIV-1 bNAbs (IgG and Fabs) to KLH, YU-2, and ZM-96 gp140 trimers, CM5 chips (Biacore) were measured as previously described (Mouquet et al., 2010). Thermodynamic parameters were determined using Eyring's analyses as previously described (Hadzhieva et al., 2017). See the Supplemental Experimental Procedures for further details.

Hydrophobicity Analyses of Fabs

Hydrophobicity of Fabs was assessed using the 8-Anilinonaphthalene-1-sulfonic acid (ANS) fluorescence probe (Sigma-Aldrich, St. Louis, MO). Fabs (at 2 μM in PBS) was incubated for 15 min at room temperature in the absence or presence of 25 μM ANS. Fluorescence intensity of ANS was measured at 500 nm after excitation at 380 nm, with excitation and emission slits set at 9 and 20 nm, respectively. The fluorescence measurements were performed using a Tecan Infinite M200 Pro multimode plate reader (Tecan, Männedorf, Switzerland). For evaluation of the specific signal of protein-bound ANS, the fluorescence intensities of ANS in the presence of Fabs were subtracted from the fluorescence of ANS in PBS only.

Molecular Dynamic Simulations

PDB coordinates were obtained from the Research Collaboratory for Structural Bioinformatics (RCSB). In all of the selected X-ray structures (PDB: 3U7W, 3NGB, 4NRY, and 4NRZ) (Diskin et al., 2011; Ofek et al., 2014; Wu et al., 2010), missing coordinates of flexible loop areas and of mutated residues were introduced using the program Modeler version (v.)9.19 (Sali and Blundell, 1993). In each case, the structure with the lowest van der Waals violations was selected as the starting structure from a set of 10 conformers generated. Molecular dynamic simulations of the antibodies were then performed as described in the Supplemental Experimental Procedures.

SUPPLEMENTAL INFORMATION

Supplemental Information includes Supplemental Experimental Procedures, six figures, and one table and can be found with this article online at https://doi.org/10.1016/j.celrep.2018.04.101.

ACKNOWLEDGMENTS

We warmly thank Florence Guivel-Benhassine (Virus & Immunity Unit, Institut Pasteur) for technical help. We also thank the NIH AIDS Reagent Program, Stéphane Petres (Recombinant proteins platform, Institut Pasteur), and Patrick England (Biophysics platform, Institut Pasteur) for contributing reagents and technical support. This work was supported by the European Research Council (ERC) – Seventh Frame-work Program (ERC-2013-StG 337146). A.K. and O.V. were supported by ERC postdoctoral fellowships (ERC-2013-StG 337146). H.M. was supported by the G5 Institut Pasteur Program and the

Milieu Intérieur Program (ANR-10-LABX-69-01). J.P. was supported by a postdoctoral fellowship from the Agence Nationale de Recherche sur le Sida et les hépatites virales (ANRS). The Fritz Lipmann Institute is a member of the Leibniz Association and is financially supported by the Federal Government of Germany and the State of Thuringia.

AUTHOR CONTRIBUTIONS

H.M. conceived the study. O.S., J.D.D., and H.M. designed experiments. J.P., A.J., C.P., C.E., J.D., A.K., V.L., O.V., T.C., T.B., M.S.S., O.O., J.D.D., and H.M. performed and analyzed experiments. O.S., O.O., J.D.D., and H.M. wrote the manuscript with contributions from all the authors.

DECLARATION OF INTERESTS

The authors declare no competing interests.

Received: January 12, 2018
Revised: March 26, 2018
Accepted: April 25, 2018
Published: May 29, 2018

REFERENCES

Acchione, M., Lipschultz, C.A., DeSantis, M.E., Shanmuganathan, A., Li, M., Wlodawer, A., Tarasov, S., and Smith-Gill, S.J. (2009). Light chain somatic mutations change thermodynamics of binding and water coordination in the HyHEL-10 family of antibodies. Mol. Immunol. *47*, 457–464.

Adhikary, R., Yu, W., Oda, M., Zimmermann, J., and Romesberg, F.E. (2012). Protein dynamics and the diversity of an antibody response. J. Biol. Chem. *287*, 27139–27147.

Alam, S.M., McAdams, M., Boren, D., Rak, M., Scearce, R.M., Gao, F., Camacho, Z.T., Gewirth, D., Kelsoe, G., Chen, P., and Haynes, B.F. (2007). The role of antibody polyspecificity and lipid reactivity in binding of broadly neutralizing anti-HIV-1 envelope human monoclonal antibodies 2F5 and 4E10 to glycoprotein 41 membrane proximal envelope epitopes. J. Immunol. *178*, 4424–4435.

Alam, S.M., Morelli, M., Dennison, S.M., Liao, H.X., Zhang, R., Xia, S.M., Rits-Volloch, S., Sun, L., Harrison, S.C., Haynes, B.F., and Chen, B. (2009). Role of HIV membrane in neutralization by two broadly neutralizing antibodies. Proc. Natl. Acad. Sci. USA *106*, 20234–20239.

Andrews, S.F., Huang, Y., Kaur, K., Popova, L.I., Ho, I.Y., Pauli, N.T., Henry Dunand, C.J., Taylor, W.M., Lim, S., Huang, M., et al. (2015). Immune history profoundly affects broadly protective B cell responses to influenza. Sci. Transl. Med. *7*, 316ra192.

Bhowmick, A., and Salunke, D.M. (2013). Limited conformational flexibility in the paratope may be responsible for degenerate specificity of HIV epitope recognition. Int. Immunol. *25*, 77–90.

Bonsignori, M., Zhou, T., Sheng, Z., Chen, L., Gao, F., Joyce, M.G., Ozorowski, G., Chuang, G.Y., Schramm, C.A., Wiehe, K., et al.; NISC Comparative Sequencing Program (2016). Maturation Pathway from Germline to Broad HIV-1 Neutralizer of a CD4-Mimic Antibody. Cell *165*, 449–463.

Bruel, T., Guivel-Benhassine, F., Amraoui, S., Malbec, M., Richard, L., Bourdic, K., Donahue, D.A., Lorin, V., Casartelli, N., Noël, N., et al. (2016). Elimination of HIV-1-infected cells by broadly neutralizing antibodies. Nat. Commun. *7*, 10844.

Chen, Y., Zhang, J., Hwang, K.K., Bouton-Verville, H., Xia, S.M., Newman, A., Ouyang, Y.B., Haynes, B.F., and Verkoczy, L. (2013). Common tolerance mechanisms, but distinct cross-reactivities associated with gp41 and lipids, limit production of HIV-1 broad neutralizing antibodies 2F5 and 4E10. J. Immunol. *191*, 1260–1275.

Chuang, G.Y., Zhang, B., McKee, K., O'Dell, S., Kwon, Y.D., Zhou, T., Blinn, J., Lloyd, K., Parks, R., Von Holle, T., et al. (2015). Eliminating antibody polyreactivity through addition of N-linked glycosylation. Protein Sci. *24*, 1019–1030.

Davenport, T.M., Gorman, J., Joyce, M.G., Zhou, T., Soto, C., Guttman, M., Moquin, S., Yang, Y., Zhang, B., Doria-Rose, N.A., et al. (2016). Somatic Hypermutation-Induced Changes in the Structure and Dynamics of HIV-1 Broadly Neutralizing Antibodies. Structure *24*, 1346–1357.

Diskin, R., Scheid, J.F., Marcovecchio, P.M., West, A.P., Jr., Klein, F., Gao, H., Gnanapragasam, P.N., Abadir, A., Seaman, M.S., Nussenzweig, M.C., and Bjorkman, P.J. (2011). Increasing the potency and breadth of an HIV antibody by using structure-based rational design. Science *334*, 1289–1293.

Diskin, R., Klein, F., Horwitz, J.A., Halper-Stromberg, A., Sather, D.N., Marcovecchio, P.M., Lee, T., West, A.P., Jr., Gao, H., Seaman, M.S., et al. (2013). Restricting HIV-1 pathways for escape using rationally designed anti-HIV-1 antibodies. J. Exp. Med. *210*, 1235–1249.

Finton, K.A., Friend, D., Jaffe, J., Gewe, M., Holmes, M.A., Larman, H.B., Stuart, A., Larimore, K., Greenberg, P.D., Elledge, S.J., et al. (2014). Ontogeny of recognition specificity and functionality for the broadly neutralizing anti-HIV antibody 4E10. PLoS Pathog. *10*, e1004403.

Goodnow, C.C., Sprent, J., Fazekas de St Groth, B., and Vinuesa, C.G. (2005). Cellular and genetic mechanisms of self tolerance and autoimmunity. Nature *435*, 590–597.

Hadzhieva, M., Pashov, A.D., Kaveri, S., Lacroix-Desmazes, S., Mouquet, H., and Dimitrov, J.D. (2017). Impact of Antigen Density on the Binding Mechanism of IgG Antibodies. Sci. Rep. *7*, 3767.

Haynes, B.F., Fleming, J., St Clair, E.W., Katinger, H., Stiegler, G., Kunert, R., Robinson, J., Scearce, R.M., Plonk, K., Staats, H.F., et al. (2005). Cardiolipin polyspecific autoreactivity in two broadly neutralizing HIV-1 antibodies. Science *308*, 1906–1908.

Jardine, J.G., Sok, D., Julien, J.P., Briney, B., Sarkar, A., Liang, C.H., Scherer, E.A., Henry Dunand, C.J., Adachi, Y., Diwanji, D., et al. (2016). Minimally Mutated HIV-1 Broadly Neutralizing Antibodies to Guide Reductionist Vaccine Design. PLoS Pathog. *12*, e1005815.

Jimenez, R., Salazar, G., Baldridge, K.K., and Romesberg, F.E. (2003). Flexibility and molecular recognition in the immune system. Proc. Natl. Acad. Sci. USA *100*, 92–97.

Kaur, H., and Salunke, D.M. (2015). Antibody promiscuity: Understanding the paradigm shift in antigen recognition. IUBMB Life *67*, 498–505.

Kelsoe, G., and Haynes, B.F. (2017). Host controls of HIV broadly neutralizing antibody development. Immunol. Rev. *275*, 79–88.

Khan, T., and Salunke, D.M. (2014). Adjustable locks and flexible keys: plasticity of epitope-paratope interactions in germline antibodies. J. Immunol. *192*, 5398–5405.

Koelsch, K., Zheng, N.Y., Zhang, Q., Duty, A., Helms, C., Mathias, M.D., Jared, M., Smith, K., Capra, J.D., and Wilson, P.C. (2007). Mature B cells class switched to IgD are autoreactive in healthy individuals. J. Clin. Invest. *117*, 1558–1565.

Krishnan, L., Lomash, S., Raj, B.P., Kaur, K.J., and Salunke, D.M. (2007). Paratope plasticity in diverse modes facilitates molecular mimicry in antibody response. J. Immunol. *178*, 7923–7931.

Krishnan, L., Sahni, G., Kaur, K.J., and Salunke, D.M. (2008). Role of antibody paratope conformational flexibility in the manifestation of molecular mimicry. Biophys. J. *94*, 1367–1376.

Kwon, Y.D., Chuang, G.Y., Zhang, B., Bailer, R.T., Doria-Rose, N.A., Gindin, T.S., Lin, B., Louder, M.K., McKee, K., O'Dell, S., et al. (2018). Surface-Matrix Screening Identifies Semi-specific Interactions that Improve Potency of a Near Pan-reactive HIV-1-Neutralizing Antibody. Cell Rep. *22*, 1798–1809.

Levy, J.A. (1998). HIV and the Pathogenesis of AIDS (ASM Press).

Li, Y., Li, H., Yang, F., Smith-Gill, S.J., and Mariuzza, R.A. (2003). X-ray snapshots of the maturation of an antibody response to a protein antigen. Nat. Struct. Biol. *10*, 482–488.

Li, M., Gao, F., Mascola, J.R., Stamatatos, L., Polonis, V.R., Koutsoukos, M., Voss, G., Goepfert, P., Gilbert, P., Greene, K.M., et al. (2005). Human immunodeficiency virus type 1 env clones from acute and early subtype B infections for standardized assessments of vaccine-elicited neutralizing antibodies. J. Virol. *79*, 10108–10125.

Liao, H.X., Chen, X., Munshaw, S., Zhang, R., Marshall, D.J., Vandergrift, N., Whitesides, J.F., Lu, X., Yu, J.S., Hwang, K.K., et al. (2011). Initial antibodies binding to HIV-1 gp41 in acutely infected subjects are polyreactive and highly mutated. J. Exp. Med. *208*, 2237–2249.

Liao, H.X., Lynch, R., Zhou, T., Gao, F., Alam, S.M., Boyd, S.D., Fire, A.Z., Roskin, K.M., Schramm, C.A., Zhang, Z., et al.; NISC Comparative Sequencing Program (2013). Co-evolution of a broadly neutralizing HIV-1 antibody and founder virus. Nature *496*, 469–476.

Liu, M., Yang, G., Wiehe, K., Nicely, N.I., Vandergrift, N.A., Rountree, W., Bonsignori, M., Alam, S.M., Gao, J., Haynes, B.F., and Kelsoe, G. (2015). Polyreactivity and autoreactivity among HIV-1 antibodies. J. Virol. *89*, 784–798.

Lorin, V., and Mouquet, H. (2015). Efficient generation of human IgA monoclonal antibodies. J. Immunol. Methods *422*, 102–110.

Lorin, V., Malbec, M., Eden, C., Bruel, T., Porrot, F., Seaman, M.S., Schwartz, O., and Mouquet, H. (2017). Broadly neutralizing antibodies suppress post-transcytosis HIV-1 infectivity. Mucosal Immunol. *10*, 829.

Manivel, V., Sahoo, N.C., Salunke, D.M., and Rao, K.V. (2000). Maturation of an antibody response is governed by modulations in flexibility of the antigen-combining site. Immunity *13*, 611–620.

Manivel, V., Bayiroglu, F., Siddiqui, Z., Salunke, D.M., and Rao, K.V. (2002). The primary antibody repertoire represents a linked network of degenerate antigen specificities. J. Immunol. *169*, 888–897.

Mohan, S., Sinha, N., and Smith-Gill, S.J. (2003). Modeling the binding sites of anti-hen egg white lysozyme antibodies HyHEL-8 and HyHEL-26: an insight into the molecular basis of antibody cross-reactivity and specificity. Biophys. J. *85*, 3221–3236.

Mohan, S., Kourentzi, K., Schick, K.A., Uehara, C., Lipschultz, C.A., Acchione, M., Desantis, M.E., Smith-Gill, S.J., and Willson, R.C. (2009). Association energetics of cross-reactive and specific antibodies. Biochemistry *48*, 1390–1398.

Mouquet, H. (2014). Antibody B cell responses in HIV-1 infection. Trends Immunol. *35*, 549–561.

Mouquet, H. (2015). Tailored immunogens for rationally designed antibody-based HIV-1 vaccines. Trends Immunol. *36*, 437–439.

Mouquet, H., and Nussenzweig, M.C. (2012). Polyreactive antibodies in adaptive immune responses to viruses. Cell. Mol. Life Sci. *69*, 1435–1445.

Mouquet, H., Scheid, J.F., Zoller, M.J., Krogsgaard, M., Ott, R.G., Shukair, S., Artyomov, M.N., Pietzsch, J., Connors, M., Pereyra, F., et al. (2010). Polyreactivity increases the apparent affinity of anti-HIV antibodies by heteroligation. Nature *467*, 591–595.

Mouquet, H., Scharf, L., Euler, Z., Liu, Y., Eden, C., Scheid, J.F., Halper-Stromberg, A., Gnanapragasam, P.N., Spencer, D.I., Seaman, M.S., et al. (2012a). Complex-type N-glycan recognition by potent broadly neutralizing HIV antibodies. Proc. Natl. Acad. Sci. USA *109*, E3268–E3277.

Mouquet, H., Warncke, M., Scheid, J.F., Seaman, M.S., and Nussenzweig, M.C. (2012b). Enhanced HIV-1 neutralization by antibody heteroligation. Proc. Natl. Acad. Sci. USA *109*, 875–880.

Muellenbeck, M.F., Ueberheide, B., Amulic, B., Epp, A., Fenyo, D., Busse, C.E., Esen, M., Theisen, M., Mordmüller, B., and Wardemann, H. (2013). Atypical and classical memory B cells produce Plasmodium falciparum neutralizing antibodies. J. Exp. Med. *210*, 389–399.

Ofek, G., Zirkle, B., Yang, Y., Zhu, Z., McKee, K., Zhang, B., Chuang, G.Y., Georgiev, I.S., O'Dell, S., Doria-Rose, N., et al. (2014). Structural basis for HIV-1 neutralization by 2F5-like antibodies m66 and m66.6. J. Virol. *88*, 2426–2441.

Prigent, J., Lorin, V., Kök, A., Hieu, T., Bourgeau, S., and Mouquet, H. (2016). Scarcity of autoreactive human blood IgA^+ memory B cells. Eur. J. Immunol. *46*, 2340–2351.

Rajpal, A., Taylor, M.G., and Kirsch, J.F. (1998). Quantitative evaluation of the chicken lysozyme epitope in the HyHEL-10 Fab complex: free energies and kinetics. Protein Sci. *7*, 1868–1874.

Rudicell, R.S., Kwon, Y.D., Ko, S.Y., Pegu, A., Louder, M.K., Georgiev, I.S., Wu, X., Zhu, J., Boyington, J.C., Chen, X., et al.; NISC Comparative Sequencing Program (2014). Enhanced potency of a broadly neutralizing HIV-1 antibody in vitro improves protection against lentiviral infection in vivo. J. Virol. *88*, 12669–12682.

Sali, A., and Blundell, T.L. (1993). Comparative protein modelling by satisfaction of spatial restraints. J. Mol. Biol. *234*, 779–815.

Scheid, J.F., Mouquet, H., Ueberheide, B., Diskin, R., Klein, F., Oliveira, T.Y., Pietzsch, J., Fenyo, D., Abadir, A., Velinzon, K., et al. (2011). Sequence and structural convergence of broad and potent HIV antibodies that mimic CD4 binding. Science *333*, 1633–1637.

Scherer, E.M., Leaman, D.P., Zwick, M.B., McMichael, A.J., and Burton, D.R. (2010). Aromatic residues at the edge of the antibody combining site facilitate viral glycoprotein recognition through membrane interactions. Proc. Natl. Acad. Sci. USA *107*, 1529–1534.

Schmidt, A.G., Xu, H., Khan, A.R., O'Donnell, T., Khurana, S., King, L.R., Manischewitz, J., Golding, H., Suphaphiphat, P., Carfi, A., et al. (2013). Preconfiguration of the antigen-binding site during affinity maturation of a broadly neutralizing influenza virus antibody. Proc. Natl. Acad. Sci. USA *110*, 264–269.

Schroeder, K.M.S., Agazio, A., Strauch, P.J., Jones, S.T., Thompson, S.B., Harper, M.S., Pelanda, R., Santiago, M.L., and Torres, R.M. (2017). Breaching peripheral tolerance promotes the production of HIV-1-neutralizing antibodies. J. Exp. Med. *214*, 2283–2302.

Shingai, M., Nishimura, Y., Klein, F., Mouquet, H., Donau, O.K., Plishka, R., Buckler-White, A., Seaman, M., Piatak, M., Jr., Lifson, J.D., et al. (2013). Antibody-mediated immunotherapy of macaques chronically infected with SHIV suppresses viraemia. Nature *503*, 277–280.

Shingai, M., Donau, O.K., Plishka, R.J., Buckler-White, A., Mascola, J.R., Nabel, G.J., Nason, M.C., Montefiori, D., Moldt, B., Poignard, P., et al. (2014). Passive transfer of modest titers of potent and broadly neutralizing anti-HIV monoclonal antibodies block SHIV infection in macaques. J. Exp. Med. *211*, 2061–2074.

Sinha, N., Mohan, S., Lipschultz, C.A., and Smith-Gill, S.J. (2002). Differences in electrostatic properties at antibody-antigen binding sites: implications for specificity and cross-reactivity. Biophys. J. *83*, 2946–2968.

Sundberg, E.J., Urrutia, M., Braden, B.C., Isern, J., Tsuchiya, D., Fields, B.A., Malchiodi, E.L., Tormo, J., Schwarz, F.P., and Mariuzza, R.A. (2000). Estimation of the hydrophobic effect in an antigen-antibody protein-protein interface. Biochemistry *39*, 15375–15387.

Tapryal, S., Gaur, V., Kaur, K.J., and Salunke, D.M. (2013). Structural evaluation of a mimicry-recognizing paratope: plasticity in antigen-antibody interactions manifests in molecular mimicry. J. Immunol. *191*, 456–463.

Thielges, M.C., Zimmermann, J., Yu, W., Oda, M., and Romesberg, F.E. (2008). Exploring the energy landscape of antibody-antigen complexes: protein dynamics, flexibility, and molecular recognition. Biochemistry *47*, 7237–7247.

Tiller, T., Tsuiji, M., Yurasov, S., Velinzon, K., Nussenzweig, M.C., and Wardemann, H. (2007). Autoreactivity in human IgG+ memory B cells. Immunity *26*, 205–213.

Tonegawa, S. (1983). Somatic generation of antibody diversity. Nature *302*, 575–581.

Verkoczy, L., and Diaz, M. (2014). Autoreactivity in HIV-1 broadly neutralizing antibodies: implications for their function and induction by vaccination. Curr. Opin. HIV AIDS *9*, 224–234.

Verkoczy, L., Diaz, M., Holl, T.M., Ouyang, Y.B., Bouton-Verville, H., Alam, S.M., Liao, H.X., Kelsoe, G., and Haynes, B.F. (2010). Autoreactivity in an HIV-1 broadly reactive neutralizing antibody variable region heavy chain induces immunologic tolerance. Proc. Natl. Acad. Sci. USA *107*, 181–186.

Verkoczy, L., Chen, Y., Bouton-Verville, H., Zhang, J., Diaz, M., Hutchinson, J., Ouyang, Y.B., Alam, S.M., Holl, T.M., Hwang, K.K., et al. (2011). Rescue of HIV-1 broad neutralizing antibody-expressing B cells in 2F5 VH x VL knockin mice reveals multiple tolerance controls. J. Immunol. *187*, 3785–3797.

Verkoczy, L., Alt, F.W., and Tian, M. (2017). Human Ig knockin mice to study the development and regulation of HIV-1 broadly neutralizing antibodies. Immunol. Rev. *275*, 89–107.

Victora, G.D., and Mouquet, H. (2018). What Are the Primary Limitations in B-Cell Affinity Maturation, and How Much Affinity Maturation Can We Drive with Vaccination? Lessons from the Antibody Response to HIV-1. Cold Spring Harb. Perspect. Biol. *10*, a029389.

Victora, G.D., and Nussenzweig, M.C. (2012). Germinal centers. Annu. Rev. Immunol. *30*, 429–457.

Wardemann, H., and Nussenzweig, M.C. (2007). B-cell self-tolerance in humans. Adv. Immunol. *95*, 83–110.

Wedemayer, G.J., Patten, P.A., Wang, L.H., Schultz, P.G., and Stevens, R.C. (1997). Structural insights into the evolution of an antibody combining site. Science *276*, 1665–1669.

Winarski, K.L., Thornburg, N.J., Yu, Y., Sapparapu, G., Crowe, J.E., Jr., and Spiller, B.W. (2015). Vaccine-elicited antibody that neutralizes H5N1 influenza and variants binds the receptor site and polymorphic sites. Proc. Natl. Acad. Sci. USA *112*, 9346–9351.

Wu, X., Yang, Z.Y., Li, Y., Hogerkorp, C.M., Schief, W.R., Seaman, M.S., Zhou, T., Schmidt, S.D., Wu, L., Xu, L., et al. (2010). Rational design of envelope identifies broadly neutralizing human monoclonal antibodies to HIV-1. Science *329*, 856–861.

Yin, J., Beuscher, A.E., 4th, Andryski, S.E., Stevens, R.C., and Schultz, P.G. (2003). Structural plasticity and the evolution of antibody affinity and specificity. J. Mol. Biol. *330*, 651–656.

Zhang, R., Verkoczy, L., Wiehe, K., Munir Alam, S., Nicely, N.I., Santra, S., Bradley, T., Pemble, C.W., 4th, Zhang, J., Gao, F., et al. (2016). Initiation of immune tolerance-controlled HIV gp41 neutralizing B cell lineages. Sci. Transl. Med. *8*, 336ra62.

Zhu, Z., Qin, H.R., Chen, W., Zhao, Q., Shen, X., Schutte, R., Wang, Y., Ofek, G., Streaker, E., Prabakaran, P., et al. (2011). Cross-reactive HIV-1-neutralizing human monoclonal antibodies identified from a patient with 2F5-like antibodies. J. Virol. *85*, 11401–11408.

Zimmermann, J., Oakman, E.L., Thorpe, I.F., Shi, X., Abbyad, P., Brooks, C.L., 3rd, Boxer, S.G., and Romesberg, F.E. (2006). Antibody evolution constrains conformational heterogeneity by tailoring protein dynamics. Proc. Natl. Acad. Sci. USA *103*, 13722–13727.